PROCEEDINGS, 43rd Workshop on Geothermal Reservoir Engineering
Stanford University, Stanford, California, February 12-14, 2018
SGP-TR-213

3D Modelling of Fracture Injection Tests Using Nonlinear Joint Elements with Application to Sigma-V

Amirhossein Kamali, Ahmad Ghassemi

Reservoir Geomechanics and Seismicity Research Center, The University of Oklahoma, Norman, OK 73019, US

ahmad.ghassemi@ou.edu

Keywords: Huff & Puff, Nonlinear Joint, Contact Element, 3D Displacement Discontinuity, Hydro-Mechanical Coupling

ABSTRACT

Heat extraction from geothermal reservoirs relies on water circulation in natural and hydraulically-induced fractures. Cold water is injected into the reservoir to extract the rock's heat upon contact as it flows through fractures. The circulation involves fracture deformation, fluid flow inside the fractures, leakoff to the matrix, fracture propagation, and heat exchange. A three-dimensional displacement discontinuity model is used along with a fluid flow model to investigate the response of fractures to different injection/extraction scenarios. Nonlinear joint elements are used to represent fracture elements in contact. A fracture propagation scheme is implemented in this model to capture the tensile propagation of natural fractures. Several numerical examples pertaining to the SIGMA-V project are presented to analyze the natural fracture behavior under different injection scenarios including simultaneous injection-extraction and "huff and puff". Our results indicate that both pre and post shut-in behaviors are affected by the fracture stiffness parameters. Fluid leakoff, on the other hand, controls the rate of propagation as well as the pressure variations inside the fracture.

1. INTRODUCTION

Extracting the geothermal energy, in a broad sense, involves injection of water into deep hot rocks and producing it at a higher temperature via production wells. The engineering and design aspects of geothermal heat extraction has evolved over the years owing to the research on this multi-physics and coupled process. This process relies on circulation of water through natural or hydraulic fractures to facilitate heat transfer between the hot rocks and the injected water. The heated water is then produced via production well(s) or the same injection well. It is evident that injection/extraction in geothermal reservoir is a complex process as it involves fracture deformation (and propagation in some cases), fluid flow inside fractures, heat exchange, pore fluid diffusion, and leakoff. The coupling between these phenomena further complicates the problem. Therefore, a thorough understanding of these concepts is required to analyze geothermal systems.

It is our objective in this paper to take a closer look at the injection/extraction problems such as "huff & puff" method which is a commonly applied technique in heat extraction from geothermal reservoirs and can also be used for reservoir characterization. This method consists of an injection interval followed by several shut-in and production intervals. The shut-in intervals assist the heat transfer between the matrix and the water at rest. In addition to the heat transfer side of this problem, hydromechanics of the circulation is of great importance as it determines the variation of fracture's width, and potential growth throughout the test. Given the low injection rates and pressures, the natural fractures/joints mostly remain mechanically closed during the huff and puff tests. Hence, the contact status and closure of natural fractures should be carefully addressed for a proper description of the huff and puff tests.

Pressure transient of huff & puff tests has been discussed in several studies using different analytical and numerical approaches (e.g. Wessling et al., 2009; Mathias et al., 2010; Safari and Ghassemi 2011). Wessling et al. (2009) employed a hydro-mechanically coupled numerical model to study the pressure transient of a huff and puff test that was performed in Hortsberg Z1 well in north-western Germany. They used a finite element model and two flow geometries in their analysis. Wessling et al. (2009) stated that the pressure transient matching that was performed in their study is not unique and a different set of parameters could possibly generate the same results. Mathias et al. (2010) developed a model by neglecting the hydro-mechanical coupling. They assumed uniform fracture pressure and aperture along the fracture which only vary with time. Mathias et al. (2010) supported these assumptions based on the observations of Wessling et al. (2009) that fracture pressure and aperture quickly become spatially uniform. Safari and Ghassemi (2011) used a fully coupled poroelastic displacement discontinuity model to examine the pressure transient of the same huff and puff test. They utilized a finite element formulation for the flow fluid and the Goodman joint model for their analysis. The integral equation solution of heat transfer and thermo-poroelasticity is provided by Ghassemi et al. (2003), Ghassemi et al. (2005), Cheng et al. (2001), and Zhou et al. (2009). These works did not consider the potential for fracture growth during the operations. However, for Sigma-V design the stability of the hydraulically induced fracture during circulation is of interest.

A fully coupled model is developed in this study using a 3D displacement discontinuity model along with an implicit finite difference scheme for the fluid flow. A 1D pressure dependent leakoff model is implemented in our model to capture the pressure variations in huff and puff tests especially during the shut-in intervals. Closed natural fractures are represented by nonlinear joint elements. This study currently does not consider heat transfer between the rock matrix and the injected water. Induced stresses due to pore fluid

diffusion is also neglected in our model. It is our objective in this paper to take a closer look at the parameters that govern the hydro-mechanical behavior of huff and puff test and the response of closed natural fractures to injection and extraction.

2. MODEL DEVELOPMENT

Circulation of water into fractured rocks is a coupled process involving rock deformation, fluid flow, and heat transfer. This section provides an overview of the steps taken to construct our model. The numerical treatment of the coupled equations is presented at the end of section.

2.1 Governing equations

The solution of an elastic body deformation should satisfy the governing equations for a given set of stress/displacement boundary conditions. The formulation of elasticity problems relies on the stress tensor partial differential equations and strain-displacement equations. The solution is then completed through a constitutive equation relating the stresses to displacements/strains. Assuming static equilibrium, isotropic and homogenous body, and linear elasticity, the constitutive equation (generalized Hooke's law) is expressed as follows:

$$\sigma_{ij} = \frac{E}{1+v}(\varepsilon_{ij} + \frac{v}{1-2v}\varepsilon_{kk}\delta_{ij}) \qquad i,j = 1,2,3 \tag{1}$$

Where σ_{ij} is the stress tensor component, E is the Young's modulus, v is the Poisson's ratio, ε_{ij} is the strain tensor component, ε_{kk} denotes summating over diagonal terms in the strain tensor, and δ_{ij} represents the Kronecker delta function. This equation relates the stresses with strains in an elastic body. Proper boundary conditions in terms of displacements and/or stresses should be prescribed in order to solve this equation.

A fluid flow model is required to find the pressure profile and the corresponding rates inside the fracture. Assuming small variations of fracture aperture in time and space so that the laminar flow assumption applies, the mass balance is written as follows:

$$\nabla_2 . q(x,y) = -\frac{\partial w(x,y,t)}{\partial t} - 2v_L + Q_{inj}\delta(X_{inj}) \tag{2}$$

Where ∇_2 is a two-dimensional divergence operator, q is the volumetric flow rate, Q_{inj} is the injection flow rate, v_L is the leak-off velocity, and w is the local fracture aperture. The term on the right-hand-side of the equation may be regarded as the coupling term as the fracture opening appears in both the mechanical equations and in the fluid flow equation. Darcy's law is used along with the cubic law to express the flow equation in terms of fluid pressure:

$$q_i = -\frac{w^3(x_i, x_j, t) l_j}{12\mu}\frac{\partial p}{\partial x_i} \tag{3}$$

In which, μ is the injection fluid viscosity, l_j is the element's size in the direction normal to the flow, p is the fluid pressure. This equation is then substituted in the mass balance equation to obtain the flow equation in terms of fluid pressure and fracture apertures.

Another key term in the flow equation is the leakoff velocity. A vast majority of fluid flow models in the fracturing context resort to a constant leakoff model such as Carter's model (Howard and Fast, 1957) due to its simplicity. However, this model is not pressure dependent and fails to predict the pressure variations properly during the extraction intervals where the pressure falls below the initial reservoir pressure. To overcome this shortcoming a pressure-dependent leakoff model is implemented in our fluid flow equation. This model is essentially the solution to the 1D fluid diffusion equation, which for a Newtonian fluid ($n = 1, k' = \mu$) could be expressed as follows:

$$\frac{\partial^2 p}{\partial x^2} = \frac{\mu\phi c_t}{k}\frac{\partial p}{\partial x} \tag{4}$$

Where ϕ is the matrix porosity, and c_t is the total compressibility. Fan and Economides (1995) proposed a solution to this PDE by dividing the reservoir into (1) disturbed and (2) undisturbed zones:

$$v_L = \frac{\varphi\eta}{2\sqrt{t-\tau}} e^{\frac{\eta^2}{4\alpha_1}} \tag{5}$$

Where η is a pressure dependent parameter that needs to be calculated iteratively, t is the global time, τ is the time when a certain location is exposed to the fluid, and α is the hydraulic diffusivity.

Joints, natural fractures, and faults are extensively studied due to their importance in the mechanical behavior of rocks and geological structures (Goodman, 1976). Closed discontinuities are often represented by contact elements. Closed elements maintain their load carrying capacity as long as their surfaces are in contact. The term "mechanically-closed" is usually used to specify that the crack surfaces are in contact. Goodman et al. (1968) introduced the term normal (shear) stiffness, Kn (Ks) to characterize the rate of change of normal (shear) stress with respect to normal (shear) displacement, Dn (Ds). Most joints exhibit nonlinearity in their normal stress-closure behavior (Brown & Scholz, 1985; Cook, 1992). The Barton-Bandis joint model (Bandis et al. 1983) is employed in this study to capture the nonlinear fracture deformations,

$$\sigma_n = \frac{K_n^0 D_n}{1 - D_n / D_n^{\max}} \tag{6}$$

Where K_n^0 is the initial normal stiffness, D_n is the normal fracture opening (i.e., normal displacement discontinuity), and $D_n^{\max}$ is the maximum allowable fracture closure. Figure 1 shows the closure plot and the NF/HF transition for a nonlinear contact element. As shown in this figure, positive D_n is regarded closure while negative is opening.

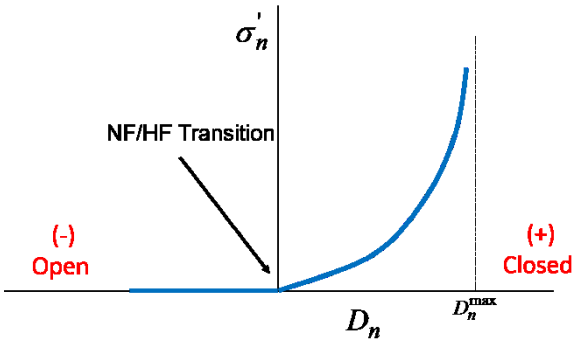

Figure 1. Closure plot for a nonlinear contact element. Normal stiffness drops to zero once the element becomes mechanically open at $\sigma_n^{'} = 0$.

Mechanically-closed fractures could transition into open fracture (see Figure 1) due to continuous water injection. Further pressurization leads to fracture propagation which needs to be addressed. We only consider the in-plane fracture propagation in this study, assuming that natural fractures are originally on the minimum stress plane. This tensile-dominated propagation is captured by enforcing a critical stress intensity criterion as follows:

$$K_I = K_{IC} \tag{7}$$

Where K_I is the mode I stress intensity factor which is calculated during the simulation, and K_{IC} is the critical stress intensity factor. This criterion is strictly applied to all the crack tip elements to ensure that the propagation pressure is not over- or underestimated at any time throughout the simulation.

2.2 Numerical Solution

As outlined in the previous section, water circulation in naturally fractured rocks is a multi-physics and coupled process. Numerical modeling is almost always adopted for solving such systems as these coupled PDEs are not amenable to analytical treatment. This section provides an overview of the numerical solutions for the fracture deformation and fluid flow equations.

Fracture deformation and stresses are calculated using displacement discontinuity method (DDM) which is proved to be a powerful tool in fracture analysis. DD is an indirect boundary element method that is used in a wide range of rock engineering problems. The original formulation of 3D DD (Salamon, 1964) is modified to account for farfield in-situ stresses, fracture stiffness and pore pressure as follows:

$$\overset{i}{\sigma_n^{\infty}} + \sum_{j=1}^{N} \overset{ij}{A_{ns1}} \overset{j}{D_{s1}} + \sum_{j=1}^{N} \overset{ij}{A_{ns2}} \overset{j}{D_{s2}} + \sum_{j=1}^{N} (\overset{ij}{A_{nn}} - \delta_{ij} K_n) \overset{j}{D_n} - p_i = 0 \tag{8-a}$$

$$\overset{i}{\sigma}{}^{\infty}_{s1}+\sum_{j=1}^{N}(\overset{ij}{A}_{s1s1}-\delta_{ij}K_s)\overset{j}{D}_{s1}+\sum_{j=1}^{N}\overset{ij}{A}_{s1s2}\overset{j}{D}_{s2}+\sum_{j=1}^{N}\overset{ij}{A}_{s1n}\overset{j}{D}_{n}=0 \tag{8-b}$$

$$\overset{i}{\sigma}{}^{\infty}_{s2}+\sum_{j=1}^{N}\overset{ij}{A}_{s2s1}\overset{j}{D}_{s1}+\sum_{j=1}^{N}(\overset{ij}{A}_{s2s2}-\delta_{ij}\overset{j}{K}_s)D_{s2}+\sum_{j=1}^{N}\overset{ij}{A}_{s2n}\overset{j}{D}_{n}=0 \tag{8-c}$$

Where σ_l^{∞} are the farfield shear and normal stresses, D denotes displacement discontinuities, A_{pq} are the elastic kernels that are constructed based on the potential functions that are introduced in Salamon (1964), and δ_{ij} is the Kronecker delta function which is defined as follows:

$$\delta_{ij}=\begin{cases}1 & i=j\\ 0 & i\neq j\end{cases} \tag{9}$$

The fluid flow equation should be discretized and solved along with the DD equations in order to find the pressure distribution in the fracture. An implicit finite difference scheme is employed to solve the fluid flow equation; central differences are used for spatial discretization whereas forward difference is used for temporal discretization. The FD equations are linked with the DD equations through the coupling term (i.e., $\partial w/\partial t$) to form the hydro-mechanically coupled system. The final form of the flow equation is expressed as follows:

$$\sum_{j=NB_{i,1}}^{NB_{i,4}}T_{ij}^{m+1}p_j-\left(\sum_{j=NB_{i,1}}^{NB_{i,4}}T_{ij}^{m+1}\right)p_i+\frac{\overset{i}{Q}_{inj}}{\Delta x\Delta y}-2\overset{i}{v}_L+\frac{\overset{i}{D}{}_n^{m+1}-\overset{i}{D}{}_n^{m}}{\Delta t}=0 \qquad i=1,2,...,N \tag{10}$$

Where T_{ij}^{m+1} is the transmissibility term evaluated at the current time step, NB denotes the neighboring element index for element i, and m is the time index. A no-flow boundary condition is prescribed at crack edges in order to solve this equation. Considering the fact that the fracture apertures and the transmissivity terms are not known in advance, an initial guess for fracture apertures is required to begin the simulation at each time step. Once the fully coupled system is solved for the pressures and fracture openings, fracture aperture values are updated. This iterative procedure is repeated within each time step until the desired tolerance is met. Leakoff velocities are also required to be calculated and updated within each time step since the leakoff rate is assumed to be pressure dependent and therefore not known. Another factor that contributes to the cost of computation is the nonlinear joint deformation; fracture stiffness is not constant and needs to be updated within the p-w coupling iterations. Moreover, contact elements experience different degrees of closure and therefore the normal stiffness varies spatially.

3. RESULTS AND DISUCSSION

A few numerical simulations are provided in this section to investigate the hydro-mechanics of circulation in geothermal applications. It is our objective to study the impact of rock, NF, fluid properties on the response of natural fractures to injection/extraction. These examples concern *huff and puff* test which is a single-well operation consisting of an injection interval and several shut-in and extraction intervals. Figure 2 shows the well and natural fracture configuration for the huff and puff test. It is assumed in this study that the well is in direct contact with the natural fracture. Simultaneous injection/extraction of water is investigated in another example to analyze fracture propagation in SIGMA-V circulation tests.

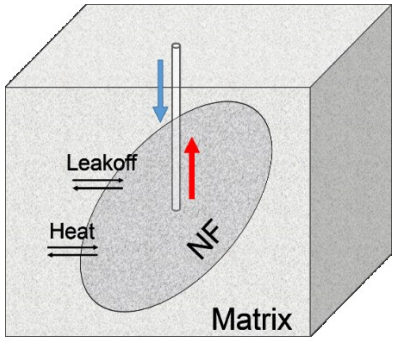

Figure 2. Huff and puff test schematic. Injection/extraction is performed via a single well. Injection of colder water and extraction of hot water are marked by blue and red arrows, respectively.

3.1 Circulation Test

Simultaneous injection and extraction of water is commonly used as a circulation test in geothermal applications. This technique involves injection of water through an injection well and producing it from an extraction well. The hydromechanics of this test is controlled by the fracture size, fracture width, well spacing, operating parameters such as injection/production rates and pressures among other factors. It is our objective in this section to analyze a circulation test using the properties that are reported in the SIGMA-V project. The initial fracture is assumed to be a penny-shaped fracture with radius of 15 *m*. The injection well is drill in the center of this fracture and well spacing is assumed to be 12 *m*. The rest of simulation parameters are listed in Table 1.

Table 1. Simulation parameters used in the circulation test.

Minimum stress, σ_{xx}	MPa	20.0	Maximum closure, D_{max}	mm	0.5
Initial pore pressure, p_o	MPa	0.0	Initial Stiffness, K_n^0	GPa/m	10.0
Matrix permeability, k	m^2	1.0×10^{-19}	Total system stiffness, c_t	1/Pa	4.5×10^{-10}
Porosity, ϕ	-	0.02	Water viscosity, μ	Pa.s	1.0×10^{-3}
Young's modulus, E	GPa	71.4	Injection rate, Q_i	m^3/s	1.0×10^{-4}
Poisson's ratio, ν	-	0.23	Extraction rate, Q_E	m^3/s	0.9×10^{-4}
Initial Aperture, w_0	mm	0.05			

The SIGMA-V circulation tests concern finding the safe operating limits of the injection/extractions rates and/or pressures to avoid fracture extension during circulation. Several attempts have been made to find the onset of fracture propagation by conducting step-rate and step-pressure tests. This example is designed to shed light on the pattern of propagation in a test where both injection and extraction wells are rate-controlled. Water is injected in the center of the fracture at a constant rate of 1.0 *l/s* and is extracted from the production well at a constant rate of 0.9 *l/s*. The net injected volume could potentially cause fracture propagation and therefore needs to be considered in the operation design. Fracture propagation patterns are investigated in this example to find the fracture trajectory in simultaneous injection/extraction tests. The test is conducted for two leakoff scenarios: case (a) with no leakoff and case (b) with a pressure-dependent leakoff. Figure 3 shows the fracture propagation pattern for the case of no leak off. It can be observed in this figure that the fracture tends to propagate farther away from the production well causing the propagation to be more noticeable in the left portion of the fracture. This, in fact, causes a deviation from the radial propagation pattern and leads to a non-circular fracture. It can be seen in this figure that the fracture has extended 7 *m* to the left of the injection well while there is no propagation near the production well. Figure 4 shows the fracture geometry at different injection times using the pressure-dependent leakoff model. It can be seen in this figure that the overall propagation pattern is similar to that of the no-leakoff example. Fracture propagation is non-uniform with more propagation closer to the injection well. The injection time to achieve propagation is, however, vastly different when leakoff is considered. This implies that neglecting leakoff could lead to erroneous estimation of fracture propagation or fracture arrival at the production well. A similar pattern of fracture geometry and propagation rate variation with production well pressure conditions has been observed in Hu and Ghassemi (2016, 2017).

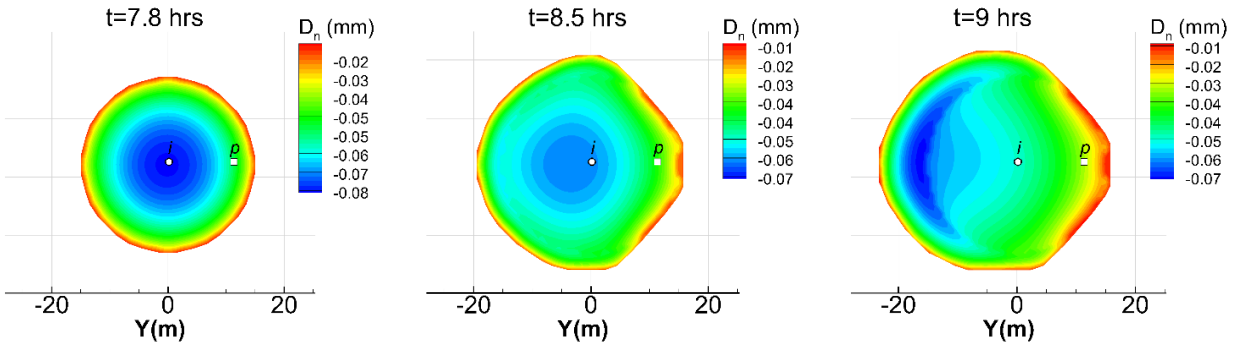

Figure 3. Fracture propagation at different injection/extraction times with no leakoff. These figures show that the fracture tends to propagate farther away from the production well.

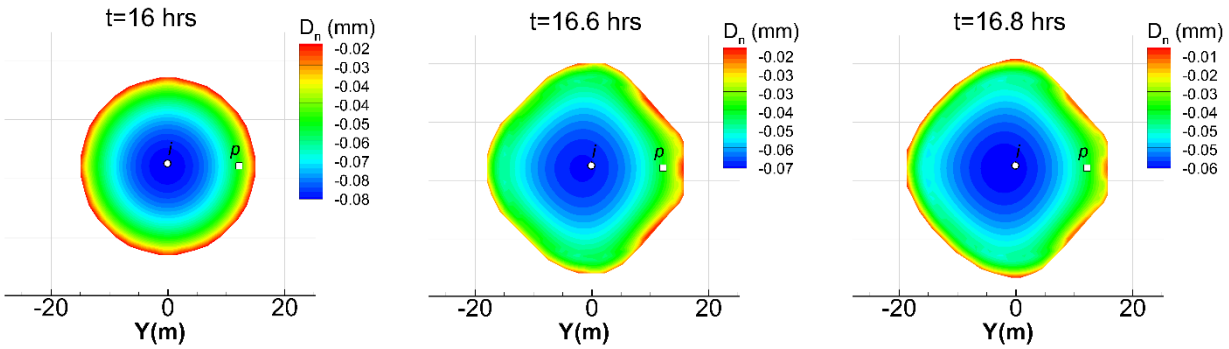

Figure 4. Fracture propagation at different injection/extraction times with pressure-dependent leakoff. These figures show that the fracture tends to propagate farther away from the production well.

3.2 Huff and Puff Test

A huff and puff scenario is simulated using nonlinear contact elements and the pressure dependent leakoff model. In this example, the water is injected directly into the closed natural fracture that is in mechanical equilibrium with the in-situ stress. The water is then produced in five successive extraction/shut-in periods. It should be mentioned that heat transfer and the corresponding thermal stresses are neglected in this example. Table 2 shows the detailed huff and puff cycle and the injection/extraction rates.

Table 2. Pump schedule for the huff and puff test.

Well Status	Rate (m^3/s)	t (hr)	Duration (hr)
Injection	0.010	0.00	1.00
Shut in	-	1.00	1.00
extraction	0.005	2.00	0.50
Shut in	-	2.50	0.25
extraction	0.005	2.75	0.50
Shut in	-	3.25	0.25
extraction	0.005	3.50	0.50
Shut in	-	4.0	0.25
extraction	0.005	4.25	0.50
Shut in	-	4.75	0.25
extraction	0.005	5.0	0.50
Shut in	-	5.50	-

The natural fracture is assumed to be a penny-shaped fracture with a radius of 100 m. The initial pore pressure and the minimum in-situ stress are 60.0 and 68.5 MPa, respectively. Rest of the simulation parameters are listed in Table 3.

Table 3. Simulation parameters used in the geothermal huff & puff test.

Minimum stress, σ_{xx}	MPa	68.5	Maximum closure, D_{max}	mm	1.20
Initial pore pressure, p_o	MPa	60.0	Initial Stiffness, K_n^0	GPa/m	5.0
Matrix permeability, k	m^2	2.5×10^{-17}	Total system stiffness, c_t	1/Pa	4.5×10^{-10}
Porosity, ϕ	-	0.05	Water viscosity, μ	Pa.s	1.0×10^{-3}
Young's modulus, E	GPa	26.0	Injection rate, Q_i	m^3/s	1.0×10^{-2}
Poisson's ratio, ν	-	0.30	Extraction rate, Q_E	m^3/s	5.0×10^{-3}
Initial Aperture, w_0	mm	0.50			

The wellbore pressure is recorded at the injection well during the huff and puff test and is shown in Figure 5. Initial pore pressure and minimum in-site stresses are shown by two dotted lines on this figure. The rate history is also shown in blue dotted line along with the

pressure profile. It can be seen in this example that the pressure increases during the first injection pressure. The slope of the pressure plot changes during the first injection period which is because of the combination of the nonlinear joint model and the pressure dependent leakoff model. The injection period is followed by a shut-in period in which the fracture pressure starts to dissipate due to the leakoff from the fracture to the matrix. The first extraction cycle begins right after the shut-in period which is marked by a steep decline in the pressure profile. It can be observed in this figure that the pressure falls below the initial pore pressure level (i.e., 60 MPa) during the first extraction period. Having said that, the pressure rises during the second shut-in period which is because of the reverse flow from the matrix into the fracture (note that the fracture pressure is below that of the infinite matrix). It is interesting to note that shut-in can cause different pressure variation patterns depending on the fluid pressure inside the fracture. In other words, shut-in causes pressure drop when fluid pressure inside the fracture is above the initial reservoir pressure (as seen during the first shut-in period) whereas it causes pressure rise when the fracture pressure is below the reservoir pressure (as in the second shut-in interval). This cycle is repeated for four more cycles before the last shut-in period. The pressure increases in the last shut-in period until it reaches the initial pore pressure level and then stabilizes. It is, of course, evident that the simulation of such process is not possible without using a pressure-dependent leakoff model which can capture the proper pressure rise/fall during the huff and puff test.

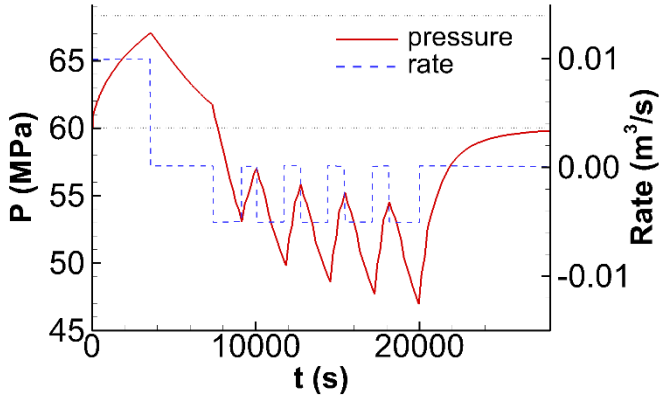

Figure 5. Pressure and rate profile at the injection/extraction well during the huff and puff test. Pressure is shown in solid red and the rate is shown in dotted blue lines. It should be noted that the fluid pressure inside the fracture drops below the initial reservoir pressure during the first extraction period. Afterwards, the fluid pressure increase during the shut-in intervals.

Figure 6 shows the pressure distribution inside the natural fracture after 1 hour of injection. It should be noticed that the fluid pressure is almost uniform with only 0.10 MPa of pressure drop from the injection well to the fracture tip. The viscous pressure drop is more noticeable in the beginning of the test when the fracture conductivity/permeability is smaller due to smaller fracture apertures. It is worth mentioning that the fracture remains mechanically closed even during the injection interval as the injection pressure does not exceed the minimum in-situ stress (i.e., 68.5 MPa).

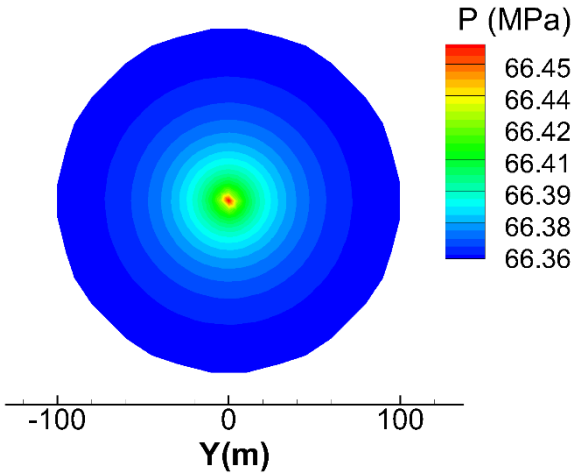

Figure 6. Pressure distribution inside the fracture at the end of the injection interval.

Fracture closure plot is shown in Figure 7 for an element in the center of the fracture. This figure shows the variation of fracture opening vs. effective stress during different injection/extraction intervals. The initial stress state (i.e., 8.5 MPa) is shown using a dashed line on the plot. It can be observed that injection causes a reduction in the effective normal stress as well as in the closure. Effective stress,

however, increases during the first shut-in interval as fluid pressure decreases due to leakoff. The effective stress and closure further increases during the first extraction interval. It is interesting to note that the impact of shut-in on the fracture pressure and the effective stress is different depending on the level of the effective stress. Shut-in increases the effective normal stress when the effective stress is below the initial stress level (i.e., fracture pressure is above the initial pore pressure). On the other hand, shut-in reduces the effective stress when the effective stress is above the initial stress level (i.e., fracture pressure is below the initial pore pressure). Water extraction always causes a reduction in the pressure and therefore increases the effective normal stress. This figure also confirms that although the effective stress approaches zero but the natural fracture never becomes mechanically-open during this particular example. This figure also indicates that the natural fracture is softer (i.e., smaller slope of the closure plot) at the end of the injection interval while being stiffer (i.e., larger slope of the closure plot) during the last extraction intervals.

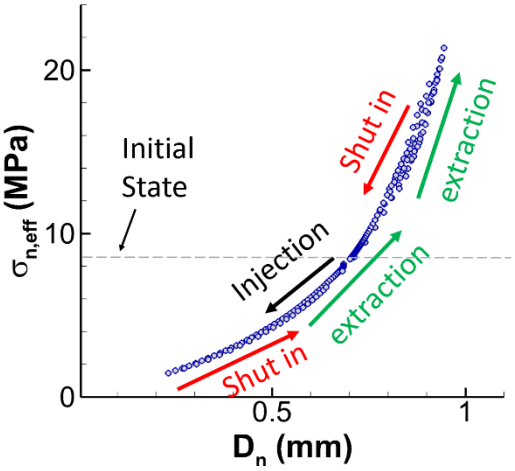

Figure 7. Nonlinear fracture closure plot. Fracture closure and opening are marked according to the well status (i.e., injection, shut-in, and extraction).

Figure 8 shows the fracture aperture at the injection/extraction well vs. time. The overall trend of the aperture profile resembles that of the fluid pressure in Figure 5. The changes of fracture aperture is directly controlled by the normal DD which itself is governed by the fracture stiffness. Higher effective normal stress (lower pressure) during the extraction intervals increases the fracture stiffness which, consequently, results in smaller changes of normal DD. Therefore, the variations of the aperture is less pronounced during the extraction period where fracture stiffness is higher. In other words, a unit change in the normal stress/pressure does not yield the same change in the normal DD when joints behave nonlinearly.

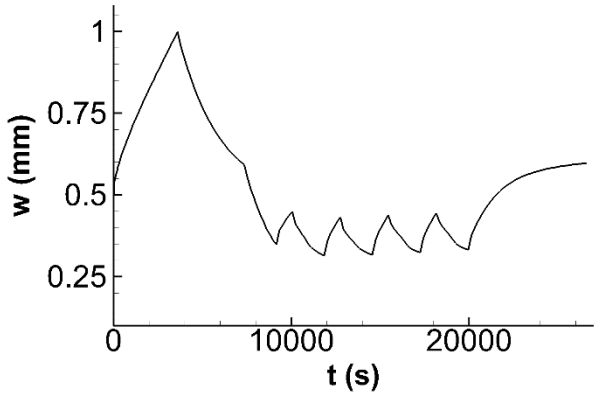

Figure 8. Variations of fracture aperture at the injection/extraction well during the huff and puff test. The changes of fracture aperture are less significant during the extraction intervals due to higher fracture stiffness which is caused by pressure drop and its corresponding increase in the effective stress.

The response of closed natural fractures and their pressure profile is governed by the rock, fluid, and fracture properties. To study the impact of fracture stiffness and matrix permeability on the pressure profile, two sensitivity analyses are conducted. The variation of fracture pressure for each case is shown in Figure 9. The matrix permeability analysis reveals that the fluid pressure increases at a lower rate during the injection interval which is due to a higher leakoff. Furthermore, the slope of pressure drop at the early stages of shut-in is relatively higher than that of the lower permeability case. Matrix permeability seems to affect the overall pressure profile including the maximum and minimum pressures during the test and the rate of pressure change. Fracture stiffness, on the other hand, appears to have

a less distinct impact on the pressure variations. It could be observed in Figure 9-b that except for the injection and the first shut-in interval, the rest of the pressure profile is almost similar for different values of fracture stiffness. These examples show that rock permeability has a significant impact on the overall pressure profile and may serve as a tuning parameter in history matching studies. Although, fracture stiffness manifests itself in the opening/closure of natural fractures (see Figure 10), it does not affect the pressure profile significantly in this particular example.

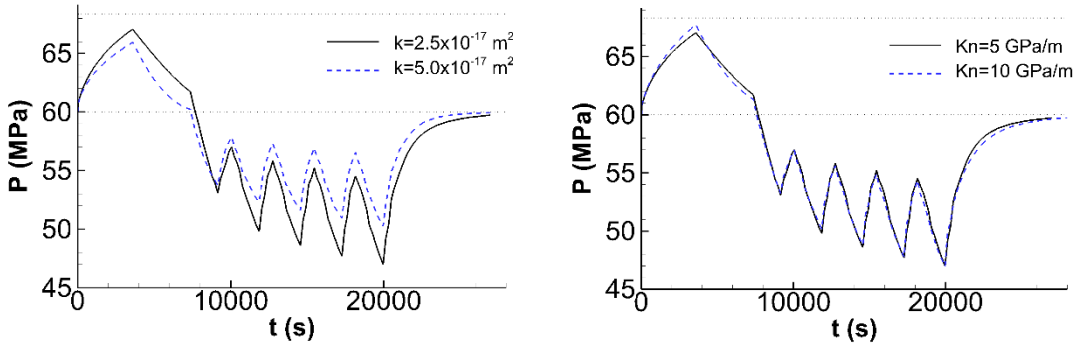

Figure 9. Evolution of fracture pressure at the injection/extraction well for (a) different matrix permeabilities (left) and (b) different fracture stiffness (right).

Fracture closure/opening is shown in Figure 10 for different values of initial stiffness. It can be observed that the fracture closure history is vastly different for different initial stiffness values. This figure shows that the fracture with higher initial stiffness approaches the open-fracture state because of the higher pressure rise in during the injection interval. It could also be observed in this figure that the effective normal stress is noticeably higher on the fracture with higher initial stiffness at the same closure level. Having said that, the pressure profiles corresponding to these cases were found to be almost similar (see Figure 9).

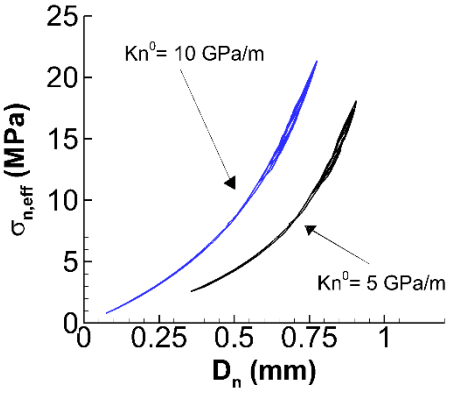

Figure 10. Fracture closure plot for different initial stiffness values.

CONLUSIONS

A hydro-mechanically coupled model is developed and used in this study to analyze the behavior of closed natural fractures in geothermal applications. This model is developed by using a 3D displacement discontinuity method to quantify fracture deformation, an implicit finite difference scheme to discretize the fluid flow equation, and nonlinear contact elements to represent the closed natural fractures. Two numerical examples are presented to analyze the pressure profile and fracture deformation during the injection/extraction intervals. The huff and puff example showed that the injection pressure profile is sensitive to the matrix permeability which controls the leakoff behavior. Fracture stiffness, on the other hand, did not impact the pressure profile significantly. The circulation test example took a closer look at the pattern of fracture propagation throughout the simulation. This example revealed that the presence of production well can potentially terminate or mitigate the fracture propagation near the production well. This, in fact, caused fracture trajectory to deviate from a circular shape. The impact of heterogeneities and natural fracture is also important and is under investigation.

ACKNOWLEDGEMENT

This work was partially based upon work supported by the U.S. Department of Energy, Office of Energy Efficiency and Renewable Energy (EERE), Office of Technology Development, Geothermal Technologies Office, under Award Number DE-AC52-07NA27344 with LLNL, Award Number DE-AC05-76RL01830 with PNNL, and Award Number DE-AC02-05CH11231 with LBNL.

REFERENCES

Bandis, S. C., Lumsden, A. C., & Barton, N. R. (1983). Fundamentals of Rock Joint Deformation. *International Journal of Rock Mechanics and Mining Sciences*, 20(6), 249-268. doi: 10.1016/0148-9062(83)90595-8.

Brown, S. R., & Scholz, C. H. (1985). Closure of random elastic surfaces in contact. *Journal of Geophysical Research: Solid Earth*, 90(B7), 5531-5545.

Cheng, A. D., Ghassemi, A., & Detournay, E. (2001). Integral equation solution of heat extraction from a fracture in hot dry rock. *International Journal for Numerical and Analytical Methods in Geomechanics*, 25(13), 1327-1338.

Cook, N. G. W. (1992). Natural Joints in Rock - Mechanical, Hydraulic and Seismic Behavior and Properties under Normal Stress. *International Journal of Rock Mechanics and Mining Sciences & Geomechanics Abstracts*, 29(3), 198-223. doi: 10.1016/0148-9062(92)93656-5.

Fan, Y., Economides, M. J. (1995). Fracturing fluid leakoff and net pressure behavior in frac & pack stimulation. In International Meeting on Petroleum Engineering. Society of Petroleum Engineers.

Ghassemi, A., Tarasovs, S., & H-D Cheng, A. (2003). An integral equation solution for three-dimensional heat extraction from planar fracture in hot dry rock. *International Journal for Numerical and Analytical Methods in Geomechanics*, 27(12), 989-1004.

Ghassemi, A., Tarasovs, S., & Cheng, A. D. (2005). Integral equation solution of heat extraction-induced thermal stress in enhanced geothermal reservoirs. *International journal for numerical and analytical methods in geomechanics*, 29(8), 829-844.

Goodman, R. E. (1976). Methods of geological engineering in discontinuous rocks.

Goodman, R. E., Taylor, R. L., & Brekke, T. L. (1968). A model for the mechanics of jointed rocks. Journal of Soil Mechanics & Foundations Div.

Howard, G. C., Fast, C. R. (1957). Optimum fluid characteristics for fracture extension. In Drilling and production practice. American Petroleum Institute.

Hu, L., Ghassemi, A., Pritchett, J., Garg, S. (2016). Laboratory Scale Investigation of Enhanced Geothermal Reservoir Stimulation. In 50th US Rock Mechanics/Geomechanics Symposium. American Rock Mechanics Association.

Hu, L., Ghassemi, A. (2017). Experimental Investigation of Hydraulically Induced Fracture Properties in Enhanced Geothermal Reservoir Stimulation. In 42nd Workshop on Geothermal Reservoir Engineering. Stanford, CA.

Mathias, S. A., Tsang, C. F., & van Reeuwijk, M. (2010). Investigation of hydromechanical processes during cyclic extraction recovery testing of a deformable rock fracture. *International Journal of Rock Mechanics and Mining Sciences*, 47(3), 517-522.

Safari, M. R., & Ghassemi, A. (2011). 3D analysis of huff and puff and injection tests in geothermal reservoirs. In Thirty-Sixth Workshop on Geothermal Reservoir Engineering (in press), Stanford University, Stanford, California.

Salamon, M. D. G. (1964). Elastic Analysis of Displacements and Stresses Induced by the Mining of Seam or Reef Deposits, Part II. Journal of the South African Institute of Mining and Metallurgy, 64(6), 197-218.

Wessling, S., Junker, R., Rutqvist, J., Silin, D., Sulzbacher, H., Tischner, T., & Tsang, C. F. (2009). Pressure analysis of the hydromechanical fracture behaviour in stimulated tight sedimentary geothermal reservoirs. *Geothermics*, 38(2), 211-226.

Zhou, X. X., Ghassemi, A., & Cheng, A. D. (2009). A three-dimensional integral equation model for calculating poro-and thermoelastic stresses induced by cold water injection into a geothermal reservoir. *International Journal for Numerical and Analytical Methods in Geomechanics*, 33(14), 1613-1640.